[Research Paper] 대한금속 · 재료학회지 (*Korean J. Met. Mater.*), Vol. 59, No. 2 (2021) pp.121-126
DOI: 10.3365/KJMM.2021.59.2.121

Fluorine-based Inductively Coupled Plasma Etching of α-Ga_2O_3 Epitaxy Film

Ji Hun Um[1], Byoung Su Choi[2], Woo Sik Jang[1], Sungu Hwang[1], Dae-Woo Jeon[3], Jin Kon Kim[1], and Hyun Cho[1,*]

[1]*Department of Nanomechatronics Engineering, Pusan National University, Busan 46241, Republic of Korea*
[2]*Department of Nano Fusion Technology, Pusan National University, Miryang 50463, Republic of Korea*
[3]*Korea Institute of Ceramic Engineering & Technology, JinJu 52851, Republic of Korea*

Abstract: α-Ga_2O_3 has the largest bandgap (~5.3 eV) among the five polymorphs of Ga_2O_3 and is a promising candidate for high power electronic and optoelectronic devices. To fabricate various device structures, it is important to establish an effective dry etch process which can provide practical etch rate, smooth surface morphology and low ion-induced damage. Here, the etch characteristics of α-Ga_2O_3 epitaxy film were examined in two fluorine-based (CF_4/Ar and SF_6/Ar) inductively coupled plasmas. Under the same source power, rf chuck power and process pressure, an Ar-rich composition of CF_4/Ar and an SF_6-rich composition of SF_6/Ar produced the highest etch rates. Monotonic increase in the etch rate was observed as the source power and rf chuck power increased in the $2CF_4$/13Ar discharges, and a maximum etch rate of ~855 Å/min was obtained at a 500 W source power, 250 W rf chuck power, and 2 mTorr pressure. A smooth surface morphology with normalized roughness of less than ~1.38 was achieved in the $2CF_4$/13Ar and $13SF_6$/2Ar discharges under most of the conditions examined. The features etched into the α-Ga_2O_3 layer using a $2CF_4$/13Ar discharge with 2 mTorr pressure showed good anisotropy with a vertical sidewall profile.

(Received December 15, 2020; Accepted January 14, 2021)

Keywords: α-Ga_2O_3 epitaxy film, SF_6/Ar, CF_4/Ar, inductively coupled plasma, etch characteristics

1. Introduction

Ga_2O_3 is one of the most promising candidates for high power electronic devices due to its large bandgap energy and high breakdown voltage characteristics. Extensive research work has recently been conducted to implement Ga_2O_3-based power electronic devices with higher critical field strength and efficiency compared to their GaN and SiC counterparts [1-3]. As a newly emerging ultra-wide bandgap semiconductor, the most stable β-phase among the five Ga_2O_3 polymorphs [4-6] is preferred, and most of the recent research has been focused on β-Ga_2O_3 field effect transistors (MOSFETs and MESFETs) and Schottky barrier diodes [7-10].

More recently, there has been increasing interest in α-phase Ga_2O_3, given its several advantages over β-Ga_2O_3. α-Ga_2O_3 has a larger bandgap (~5.3 eV) and higher Baliga's figure-of-merit (FOM) compared to β-Ga_2O_3 [11,12]. It has the same corundum crystal structure as a sapphire substrate with the smallest lattice mismatch among the polymorphs of Ga_2O_3, and this allows high quality, large area epitaxial growth using various growth techniques such as Halide Vapor Phase Epitaxy (HVPE), Mist Chemical Vapor Deposition (mist-CVD), and Molecular Beam Epitaxy (MBE) [13-15]. In addition, tuning of the bandgap energy from ~3.7 to ~8.75 eV is possible through alloying with α-In_2O_3 and α-Al_2O_3 [16,17]. For example, a α-Ga_2O_3 Schottky barrier diode showed a lower on-resistance of 0.1 mΩ·cm^2 compared a β-Ga_2O_3 Schottky rectifier [18].

When fabricating α-Ga_2O_3-based microelectronic devices such as MOSFETs, Schottky barrier diodes, UV detectors, and UV-LEDs, a patterning process that accurately transfers various features into the α-Ga_2O_3 layer is essential. The pattern transfer can be carried out by either wet etching or dry etching. There have been some reports on the wet etching of β-Ga_2O_3 [19-23], but it is very difficult to produce

- 엄지훈: 석사과정, 최병수: 박사과정, 장우식: 학부생, 황승구·김진곤·조현: 교수, 전대우: 연구원
**Corresponding Author:* Hyun Cho
[Tel: +82-51-510-6113, E-mail: hyuncho@pusan.ac.kr]

practical etch rates with conventional wet etching at low temperature, because of the high chemical inertness of Ga_2O_3. Moreover, the isotropic nature of wet etching makes it incapable of performing high resolution pattern transfers of sub-micron device features [24,25]. Dry etching techniques utilizing a high density plasma source, such as inductively coupled plasma (ICP) and electron cyclotron resonance (ECR), have been shown to produce higher etch rates for GaN and SiC compared to conventional reactive ion etching (RIE) and chemically-assisted ion beam etching (CAIBE) [26-30]. In addition, the ion-induced damage can be minimized because of the ability to control ion flux and ion energy separately. Therefore, high density plasma etch techniques are the preferred patterning technique for α-Ga_2O_3-based microelectronic devices. However, there have been only a few reports on the high density plasma etching of α-Ga_2O_3 epitaxy film [31].

In this work, we report a parametric study on the etch characteristics of α-Ga_2O_3 epitaxy film grown on sapphire in two fluorine-based (CF_4/Ar and SF_6/Ar) inductively coupled plasmas. The effects of plasma composition, ICP source power, rf chuck power and process pressure on the etch rate, surface morphology and etch anisotropy were studied.

2. Experimental

α-Ga_2O_3 epitaxy films were grown on 2 inch diameter c-axis sapphire substrates using the horizontal halide vapor phase epitaxy (HVPE) method. During the growth process, Ga metal, HCl and O_2 gases were used as precursors and the substrate temperature was maintained at 470 ºC, and the typical thickness of the grown α-Ga_2O_3 epitaxy films were ~1 μm [32,33]. The surface of the grown α-Ga_2O_3 epitaxy film was chemically cleaned and then, the samples were patterned with AZ5214 photoresist and Nickel. The etching of the α-Ga_2O_3 epitaxy film was performed in a planar type inductively coupled plasma (ICP) source operating at 13.56 MHz and power up to 1000 W, and the samples were thermally bonded to a Si carrier wafer that was mechanically clamped to a He backside-cooled, rf-powered (13.56 MHz, up to 450W) chuck. CF_4/Ar and SF_6/Ar ICP discharges with a total gas load of 15 standard cubic centimeters per minute (sccm) were employed to etch the α-Ga_2O_3, and the process pressure was varied from 2-20 mTorr during etching. After removal of the mask layer, the etch rate, surface morphology and anisotropy of the etched features were characterized by stylus profilometry, tapping mode atomic force microscopy (AFM) and field-emission scanning electron microscopy (FE-SEM), respectively.

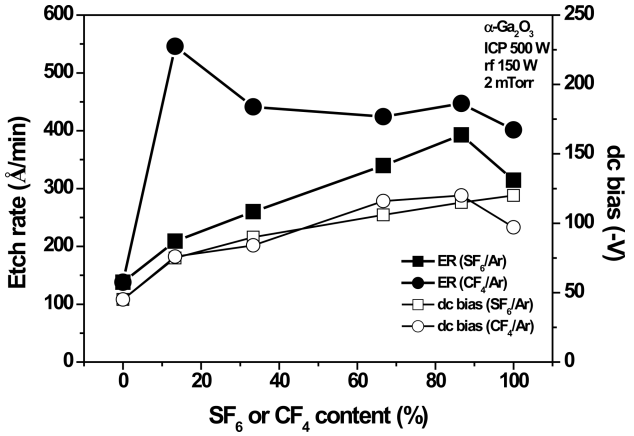

Fig. 1. α-Ga_2O_3 etch rate as a function of plasma composition in CF_4/Ar and SF_6/Ar ICP discharges (500 W source power, 150 W rf chuck power, 2 mTorr pressure).

3. Results and Discussion

Figure 1 shows the plasma composition dependence of the α-Ga_2O_3 etch rate in CF_4/Ar and SF_6/Ar ICP discharges under fixed ICP source power (500 W), rf chuck power (150 W) and pressure (2 mTorr) conditions. In the SF_6/Ar discharges, the etch rate initially increases as the SF_6 content increases due to the increase in reactive fluorine radical density in the plasma. After reaching a maximum value of ~392.8 Å/min at 86.7% SF_6 content, the etch rate decreases in pure SF_6 discharge due to the reduced ion-assisted removal of the GaF_x etch products (presumably GaF_3 ; b.p. 1000 ºC) formed on the surface. In the case of CF_4/Ar discharges, as the CF_4 content increased to 13.3 %, the α-Ga_2O_3 etch rate rapidly increased by a factor of ~4 compared to the pure Ar discharge. This is attributed to the formation of GaF_x etch products enhanced by the CF_4 addition and balanced with subsequent ion-assisted desorption. However, further increases in the CF_4 content led to a reduction in the etch rate, most likely due to the build-up of a fluorinated selvedge layer with low volatility on the surface.

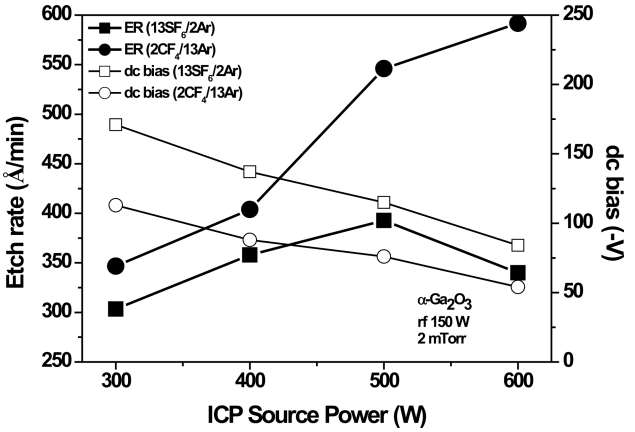

Fig. 2. α-Ga_2O_3 etch rate as a function of ICP source power in $2CF_4$/13Ar and $13SF_6$/2Ar ICP discharges (150 W rf chuck power, 2 mTorr pressure).

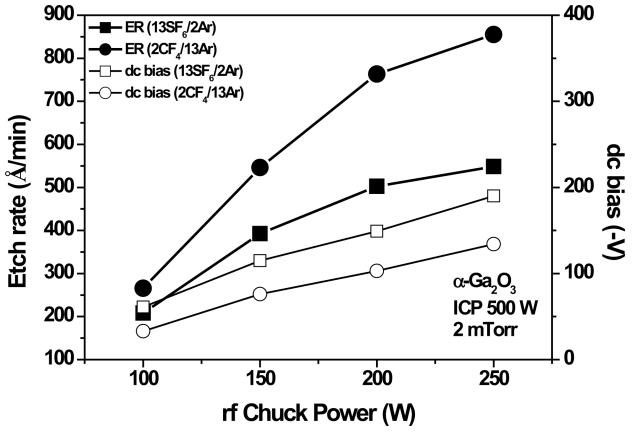

Fig. 3. α-Ga_2O_3 etch rate as a function of rf chuck power in $2CF_4$/13Ar and $13SF_6$/2Ar ICP discharges (500 W source power, 2 mTorr pressure).

Figure 2 shows the effect of ICP source power on the α-Ga_2O_3 etch rate in the $2CF_4$/13Ar and $13SF_6$/2Ar discharges, which produced the highest etch rates among the composition conditions presented in Figure 1. In the $2CF_4$/13Ar discharges, the etch rate showed a strong dependence on the source power and higher etch rates were obtained compared to the $13SF_6$/2Ar discharges. The α-Ga_2O_3 etch rate continuously increased as the source power increased, due to the increased reactive fluorine radical density and ion flux in the discharge. A maximum etch rate of ~592 Å/min was obtained at 600 W source power. A similar trend was observed in the $13SF_6$/2Ar discharges up to a source power of 500 W. The decrease in the etch rate at 600 W source power is most likely related to a decrease in ion energy caused by an increase in the source power.

The α-Ga_2O_3 etch rate as a function of the rf chuck power in the $2CF_4$/13Ar and $13SF_6$/2Ar discharges is shown in Figure 3. During etching, the ICP source power and pressure were maintained at 500 W and 2 mTorr, respectively. In both the $2CF_4$/13Ar and $13SF_6$/2Ar discharges, the etch rate monotonically increased as the rf chuck power increased, indicating the etch reaction under these conditions is dominated by the physical component of the etching. Increasing the rf chuck power increases the energy of the ions in the

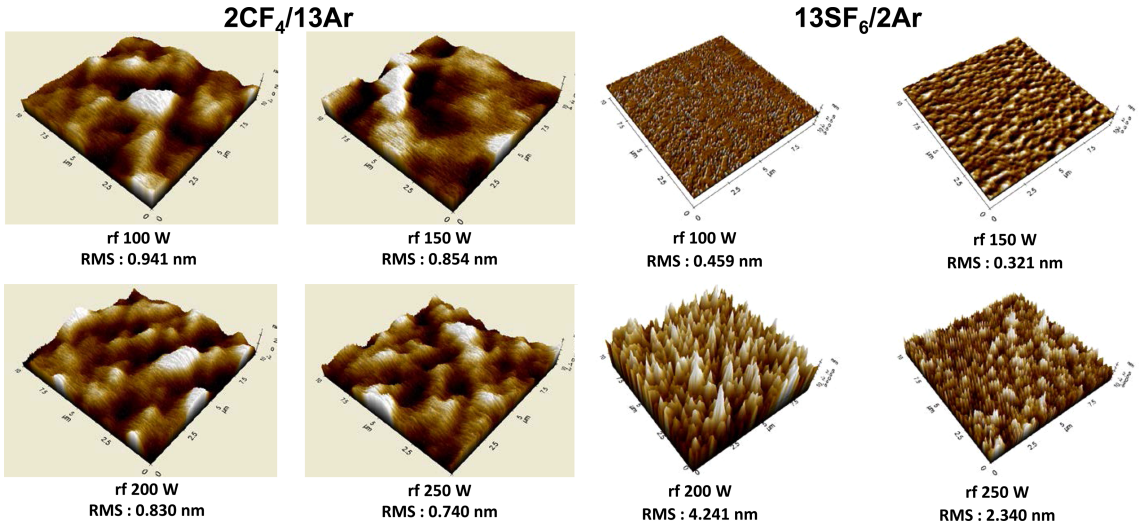

Fig. 4. AFM surface scan images of α-Ga_2O_3 etched in $2CF_4$/13Ar and $13SF_6$/2Ar ICP discharges with variation of rf chuck power (500 W source power, 2 mTorr pressure).

discharges (Ar^+ and CF_3^+ in the $2CF_4$/13Ar, and Ar^+ and SF_5^+ in the $13SF_6$/2Ar, respectively) [34-36] and improves the ion-assisted removal of nonvolatile GaF_x etch products. Then this leads to an increase in the etch rate. Maximum etch rates of ~855 Å/min and ~548.3 Å/min were obtained with a moderate rf chuck power (250 W) in the $2CF_4$/13Ar and $13SF_6$/2Ar discharges, respectively.

Figure 4 shows the AFM surface scan images of the α-Ga_2O_3 epitaxy films etched in the $2CF_4$/13Ar and $13SF_6$/2Ar discharges with variation of rf chuck power at a fixed source power (500 W) and pressure (2 mTorr). The determined normalized roughness is presented in Figure 5. Etch depth in each sample was maintained at ~2000 Å and the root-mean-square (RMS) roughness of the unetched α-Ga_2O_3 control sample was ~0.68 nm. The α-Ga_2O_3 samples etched in the $2CF_4$/13Ar discharges show almost the same surface roughness as the unetched control sample (normalized roughness in the range of 1.08-1.38) over the entire rf chuck power conditions examined. This is a typical feature of a physically-dominated etch process where the angular dependence of the ion milling removes sharp surface features faster [37].

For the $13SF_6$/2Ar discharge, the α-Ga_2O_3 samples etched at a low rf chuck power of 150 W or less showed smoother surface morphology than the unetched control sample, while

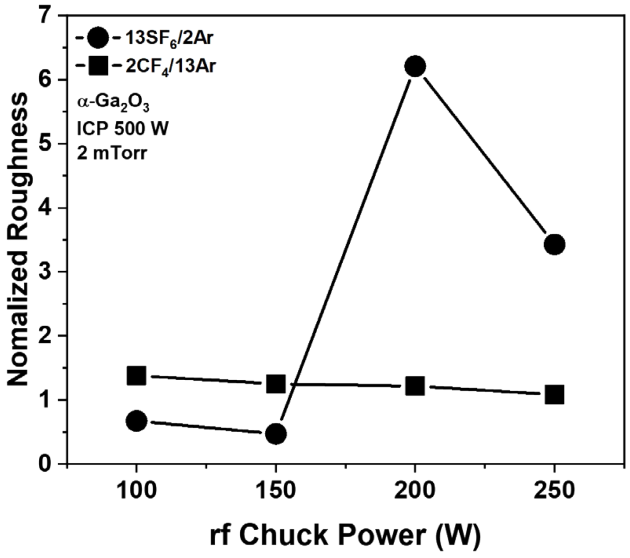

Fig. 5. Dependence of α-Ga_2O_3 normalized etched surface roughness on rf chuck power in $2CF_4$/13Ar and $13SF_6$/2Ar ICP discharges (500 W source power, 2 mTorr pressure).

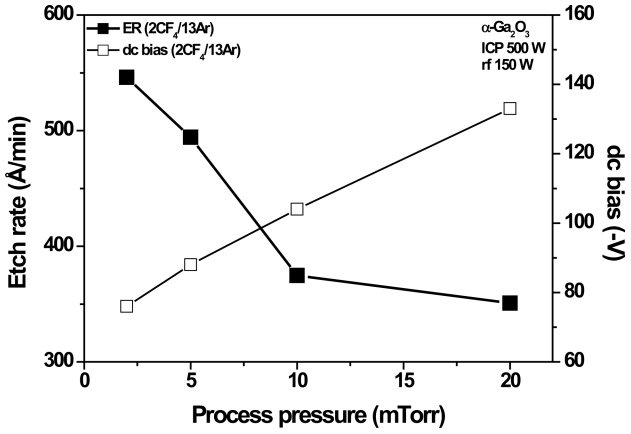

Fig. 6. α-Ga_2O_3 etch rate as a function of process pressure in $2CF_4$/13Ar ICP discharges (500 W source power, 150 W rf chuck power).

significant surface roughening was observed at rf chuck powers above 200 W, most likely due to the inhomogeneous removal of GaF_x etch products or surface atoms by enhanced ion bombardment.

The effect of process pressure on the α-Ga_2O_3 etch rate in the $2CF_4$/13Ar discharge is shown in Figure 6. As the process pressure increases, the etch rate continues to decrease due to the reduced physical contribution to the etching. This is because the increase in the process pressure reduces the mean-free-path of ions in the discharge and increases the energy loss of ions impinging on the surface.

Figure 7 shows the SEM cross-sectional images of the

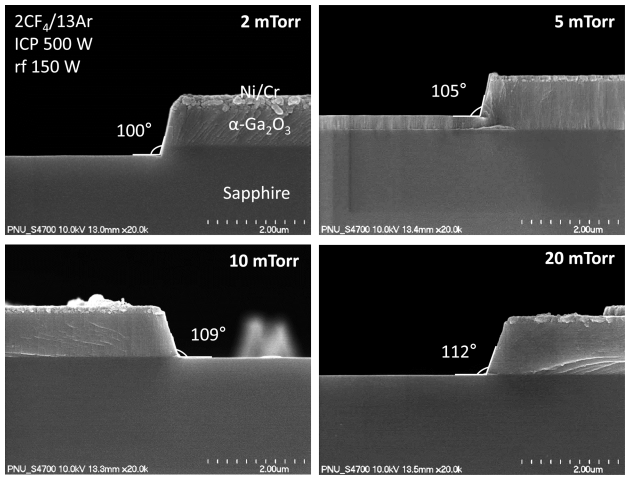

Fig. 7. Cross-sectional SEM micrographs of features etched into α-Ga_2O_3 using $2CF_4$/13Ar ICP discharges (500 W source power, 150 W rf chuck power).

features etched into the α-Ga_2O_3 layer under the same conditions presented in Fig. 6. Please note that the Ni mask layer is still in place. In the case of the feature etched under the lowest pressure condition of 2 mTorr, it can be seen that a highly anisotropic pattern transfer with a quite vertical sidewall (~100 °) was achieved due to the ion-assisted nature of the etching. But as the process pressure increased, the frequency of normal incidence of ions was reduced due to the increased collisions with other ions or neutrals in the discharge, resulting in an increased off-angle from the vertical.

4. Summary and Conclusions

High density plasma etching of α-Ga_2O_3 epitaxy film was performed in CF_4/Ar and SF_6/Ar inductively coupled plasmas and the effect of plasma composition, ICP source power, rf chuck power and process pressure on the etch rate, surface morphology and etch profile was examined. In the CF_4/Ar discharges with low CF_4 content, a significant increase in the etch rate was observed due to the synergetic effect between the physical and chemical component of the etching. However, the etch rate generally increased with increasing SF_6 content in the SF_6/Ar. The etch rate showed a stronger dependence on the source power and rf chuck power in the $2CF_4$/13Ar discharge compared to the $13SF_6$/2Ar discharge. The $2CF_4$/13Ar discharge produced higher etch rates under all conditions examined, and maximum etch rates of ~855 Å/min and ~548.3 Å/min were obtained in the $2CF_4$/13Ar and $13SF_6$/2Ar discharges, respectively at 500 W source power, 250 W rf chuck power, and 2 mTorr pressure. The α-Ga_2O_3 surfaces etched either in the $2CF_4$/13Ar or low rf chuck powered (less than 150 W) $13SF_6$/2Ar discharge showed a smooth morphology. Highly anisotropic pattern transfer was performed in the $2CF_4$/13Ar discharge with low pressure (2 mTorr) due to the ion-assisted nature of the etching, and the etch rate and etch anisotropy were reduced as process pressure increased. The results of this work show that fluorine-based ICP etching would be a reasonable choice for fabricating a α-Ga_2O_3 device structure with a smooth surface morphology.

REFERENCES

1. S. J. Pearton, F. Ren, M. Tadjer, and J. Kim, *J. Appl. Phys.* **124**, 220901 (2018).
2. K. Konishi, K. Goto, H. Murakami, Y. Kumagai, A. Kuramata, S. Yamakoshi, and M. Higashiwaki, *Appl. Phys. Lett.* **110**, 103506 (2017).
3. M. Higashiwaki, H. Murakami, Y. Kumagai, and A. Kuramta, *Jpn. J. Appl. Phys.* **55**, 1202A1 (2016).
4. S. I. Stepanov, V. I. Nikolaev, V. E. Bougrow, and A. E. Romanov, *Rev. Adv. Mater. Sci.* **44**, 63 (2016).
5. C. Roy, V. G. Hill, and B. F. Osborn, *J. Am. Chem. Soc.* **74**, 719 (1952).
6. H. He, R. Orlando, M. A. Blanco, R. Pandey, E. Amzallag, I. Baraille, and M. Rerat, *Phys. Rev. B* **74**, 195123 (2006).
7. M. Orita, H. Ohta, and M. Hirano, *Appl. Phys. Lett.* **77**, 4166 (2000).
8. A. Kuramata, K. Koshi, S. Watanabe, Y. Yamaoka, T. Masui, and S. Yamakoshi, *Jpn. J. Appl. Phys.* **55**, 1202A2 (2016).
9. J. H. Kim, M. A. Mastro, M. J. Tadjer, and J. H. Kim, *ACS Appl. Mater. Interfaces* **9**, 21322 (2017).
10. A. J. Green, K. D. Chabak, E. R. Heller, R. C. Fitch, M. Baldini, A. Fiedler, K. Irmscher, G. Wagner, Z. Galazka, S. E. Tetlak, A. Crespo, K. Leedy, and G. H. Jessen, *IEEE Electron Device Lett.* **37**, 902 (2016).
11. S. J. Pearton, J. Yang, P. H. Cary, F. Ren, J. H. Kim, M. Tadjer, and M. A. Mastro, *Appl. Phys. Rev.* **5**, 011301 (2018).
12. K. Kaneko, I. Kakeya, S. Komori, and S. Fujita, *J. Appl. Phys.* **113**, 233901 (2013).
13. J. H. Park, R. MxClintock, and M. Razeghi, *Semicond. Sci. Technol.* **34**, 08LT01 (2019).
14. Y. Yao, S. Okur, L. A. M. Lyle, G. S. Tompa, T. Salagi, N. Sbrockey, R. F. Davis, and L. M. Porter, *Mater. Res. Lett.* **6**, 268 (2018).
15. M. Oda, R. Tokuda, H. Kambara, T. Tanikawa, T. Sasaki, and T. Hitora, *Appl. Phys. Express* **9**, 021101 (2016).
16. K. Kanaeko, S. Fujita, and T. Hitora, *Jpn. J. Appl. Phys.* **57**, 02CB18 (2018).
17. S.-H. Choe, Y.-J. Park, Y.-S. Kim, B.-C. Cha, S.-B. Heo, S. Yoon, Y.-M. Kong, and D. Kim, *Korean J. Met. Mater.* **58**, 793 (2020).
18. S. Fujita, M. Oda, K. Kaneko, and T. Hitora, *J. Appl. Phys.* **55**, 1202A3 (2016).

19. S. Jang, S. Jung, K. Beers, J. Yang, F. Ren, A. Kuramata, S. J. Pearton, and K. H. Baik, *J. Alloys Compd.* **731**, 118 (2018).
20. T. Oshima, T. Okuno, N. Arai, Y. Kobayashi, and S. Fujuta, *Jpn. J. Appl. Phys.* **48**, 040208 (2009).
21. H. Okumura and T. Tanaka, *Jpn. J. Appl. Phys.* **58**, 120902 (2019).
22. Y. Zhang, A. Mauze, and J. S. Speck, *Appl. Phys. Lett.* **115**, 013501 (2019).
23. S. Ohira and N. Arai, *Phys. Stat. Sol. C* **5**, 3116 (2008).
24. D. Zhuang and J. H. Edgar, *Mater. Sci. Eng. R* **48**, 1(2005).
25. F. Ren, M. Hong, J. P. Mannaerts, J. R. Lothian, and A. Y. Cho, *J. Electrochem. Soc.* **144**, L239 (1997).
26. H. Cho, C. B. Vartuli, S. M. Donovan, J. D. Mackenzie, C. R. Abernathy, S. J. Pearton, R. J. Shul, and C. Constantine, *J. Electr. Mater.* **27**, 166 (1998).
27. H. Cho, K. P. Lee, P. Leerungnawarat, S. N. G. Chu, F. Ren, S. J. Pearton, and C.-M. Zetterling, *J. Vac. Sci. Technol. A* **19**, 1878 (2001).
28. J. M. Lee, K. M. Chang, S. W. Kim, C. Huh, I. H. Lee, and S. J. Park, *J. Appl. Phys.* **87**, 7667 (2000).
29. D. Basak, M. Verdu, M. T. Montojo, M. A. Sanchez-Garcia, F. J. Sanchez, E. Munoz, and E. Calleja, *Semicond. Sci. Technol.* **12**, 1654 (1997).
30. L. Y. Kuritzky, D. L. Becerra, A. S. Abbas, J. Nedy, S. Nakamura, S. P. DenBaars, and D. A. Cohen, *Semicond. Sci. Technol.* **31**, 075008 (2016).
31. Z. Jian, Y. Oshima, S. Wright, K. Owen, and E. Ahmadi, *Semicond. Sci. Technol.* **34**, 03506 (2019).
32. H. Son, Y. J. Choi, Y. J. Lee, M. J. Lee, J. H. Kim, S. W. Kim, Y. H. Ra, T. Y. Lim, J. Hwang, and D. W. Jeon, *J. Korean Cryst. Growth Cryst. Technol.* **28**, 135 (2018).
33. H. Son, Y. J. Choi, Y. J. Lee, J. H. Kim, S. W. Kim, Y. H. Ra, T. Y. Lim, J. Hwang, and D. W. Jeon, *J. Korean Cryst. Growth Cryst. Technol.* **29**, 173 (2019).
34. K. Kim, A. Efremov, J. Lee, K. H. Kwon, and G. Y. Yeom, *J. Vac. Sci. Technol. A* **33**, 031601 (2015).
35. T. Sreenidhi, K. Baskar, A. DasGupta, and N. DasGupta, *Semicond. Sci. Technol.* **23**, 125019 (2008).
36. S. J. Oh, H. C. Lee, and C. W. Chung, *Phys. Plasmas* **24**, 013512 (2017).
37. H. Cho, K. P. Lee, Y. B. Hahn, E. S. Lambers, and S. J. Pearton, *Mater. Sci Eng. B* **67**, 145 (1999).